NASA Technical Memorandum 81216

Experimental Studies of Scale Effects on Oscillating Airfoils at Transonic Speeds

Sanford S. Davis

July 1980

National Aeronautics and
Space Administration

NASA Technical Memorandum 81216

Experimental Studies of Scale Effects on Oscillating Airfoils at Transonic Speeds

Sanford S. Davis, Ames Research Center, Moffett Field, California

National Aeronautics and
Space Administration

Ames Research Center
Moffett Field, California 94035

EXPERIMENTAL STUDIES OF SCALE EFFECTS ON OSCILLATING AIRFOILS AT TRANSONIC SPEEDS

Sanford S. Davis
Aerodynamic Research Branch
Aerodynamics Division
Ames Research Center, NASA
Moffett Field, California 94035, U.S.A.

SUMMARY

Experimental data are presented on the effect of Reynolds number on unsteady pressures induced by the pitching motion of an oscillating airfoil. Scale effects are discussed with reference to a conventional airfoil (NACA 64A010) and a supercritical airfoil (NLR 7301) at mean-flow conditions that support both weak and strong shock waves. During the experiment the Reynolds number was varied from 3×10^6 to 12×10^6 at a Mach number and incidence necessary to induce the required flow. Both fundamental frequency and complete time history data are presented over the range of reduced frequencies that is important in aeroelastic applications. The experimental data show that viscous effects are important in the case of the supercritical airfoil at all flow conditions and in the case of the conventional airfoil under strong shock-wave conditions. Some frequency-dependent viscous effects were also observed.

LIST OF SYMBOLS

C_p	static pressure coefficient, (P - PINF)/QINF
$C_p(x,t)$	instantaneous pressure coefficient
$C_{p,\alpha}(x)$	first harmonic complex amplitude of the unsteady pressure, per radian
c	chord of wing, 0.5 m
exp(-iωt)	cos ωt - i sin ωt
f	frequency, Hz, fT = 1
$I_q(t)$	qth moment of the instantaneous pressure coefficient
$I_{0,\alpha}$	first harmonic complex amplitude of the upper surface loading, per radian
k	reduced frequency, ωc/2U
M	free-stream Mach number
P(x,t)	instantaneous pressure, N/m^2
PINF	free-stream static pressure, N/m^2
QINF	free-stream dynamic pressure, N/m^2
Re	chord Reynolds number
T	period of the motion, sec
t	time, sec
U	free-stream velocity, m/sec
x	distance along airfoil, m
α	complex amplitude of the unsteady angle of attack
α_m	mean angle of attack
$\alpha(t)$	instantaneous angle of attack
ω	radian frequency, 1/sec

Complex notations:

Im[ ]	imaginary part of [ ]
Mag[ ]	magnitude of [ ]
Ph[ ]	phase of [ ], deg
Re[ ]	real part of [ ]

1. INTRODUCTION

Scale effects have been considered an important element in aerodynamics research for many years. In early experimental studies of steady transonic flows in the 1940s, the Reynolds number, as it affected the state of the boundary layer approaching a shock wave, was recognized as a critical parameter (Ref. 1). In the 1950s the boundary-layer-trip technique was developed to simulate high Reynolds number flows in the wind tunnel (Ref. 2). With the development of thicker and more highly loaded airfoil sections in the 1960s, more complicated scale effects due to local flow separations were discovered (Ref. 3), and extensive experimental programs were developed to quantify these viscous interactions (Refs. 4, 5). Even today, a concerted effort is under way to understand the effect of Reynolds number on modern supercritical airfoil sections (see Gessow's introductory remarks to a recent NASA conference, Ref. 6).

In the field of unsteady transonic aerodynamics, the scale effect has hardly been seriously considered, either experimentally or analytically. In the original chapter on boundary-layer effects in the AGARD Manual on Aeroelasticity (Ref. 7), the authors of that work found no studies that considered the coupling of a boundary layer to the unsteady-pressure field. In Jones' review of unsteady aerodynamics in 1963 (Ref. 8), the need for such research was reiterated; current review articles continue to cite the need for such research (Refs. 9, 10).

Recently, numerical solutions to the Navier-Stokes equations were applied to unsteady transonic flow problems (Refs. 11-13). They were used to model passively excited oscillations where good qualitative agreement with experiment was demonstrated. Computations for a forced oscillation problem, including viscous effects, were reported in Ref. 14. All these codes, mostly concerned with mild transonic interactions where simple turbulence models suffice, are limited by long executing times, even on powerful computers. Future applications of the numerical method, guided by experimental data, better turbulence models,

and the availability of faster computers will certainly contribute to our understanding of scale effects on unsteady aerodynamic response.

Experimentally, Tijdeman (Ref. 15) analyzed some of the NLR oscillatory data for scale effect. He accounted for the boundary layer by including the displacement effect in the calculated pressure distributions. For subsonic flows, his results show that thickness and boundary-layer effects tend to counteract one another in the sense that measured unsteady-pressure distributions tend to follow classical flat-plate theory. For transonic flows, his analysis showed that the boundary layer had a profound effect on both the mean shock-wave location and the characteristic unsteady-pressure peak at the mean shock locations. Tijdeman showed that inviscid theories are inadequate for predicting unsteady transonic flows, but his data, measured in an atmospheric wind tunnel, did not address the effect of Reynolds number directly. Similar comparisons and conclusions were reported by Grenon et al. (Ref. 16) in their oscillating flap studies.

In this paper experimental data from tests in the 11- by 11-Foot Transonic Wind Tunnel at Ames Research Center are used to illustrate the importance of scale effects on the unsteady aerodynamics of both conventional and supercritical airfoils. First, the integrated upper-surface unsteady-pressure distributions are used to assess global variations (Sec. 3.1). More detailed information is presented with the aid of the fundamental frequency pressure data (Sec. 3.2), and ultimately with the instantaneous time histories (Sec. 3.3). Many of the effects involve complex unsteady viscous interactions that are not yet completely understood nor easily modeled; as a result, theoretical comparisons will be restricted to linearized, inviscid, unsteady aerodynamic theory.

2. EXPERIMENTAL APPARATUS AND TEST CONDITIONS

The experiment was conducted during the early part of 1978. The 11- by 11-Foot Transonic Wind Tunnel is a continuous flow facility that can be pressurized between 50 and 200 kPa for independent control of Mach and Reynolds number. The test wings — an NACA 64A010 conventional airfoil section and an NLR 7301 supercritical airfoil section — were mounted between two floor-to-ceiling splitter plates installed in the 3.35- by 3.35-m slotted test section. The 0.5-m-chord by 1.35-m-span wings were fabricated from a lightweight graphite-epoxy composite material. A sketch of the test apparatus is shown in Fig. 1, and a complete description of the test hardware, motion generators, and models is given in Ref. 17. The chord Reynolds number range was approximately 3×10^6 to 12×10^6. No boundary-layer trips were used in this test.

The data reported in this paper form a small portion of the extensive data base that was collected during the test. Some of the data were previously reported in Refs. 18 and 19, and a discussion of the method used to acquire and validate the unsteady data is presented in Ref. 20. The data subset relating to scale effects is presented in Table 1. Two broad categories are represented: conditions 1 to 3 represent attached flows and conditions 4 and 5 are examples of separated flows. As will be shown presently, both classes of flows can exhibit scale effects, with the separated flow data indicating a more erratic behavior.

3. PRESENTATION OF DATA AND DISCUSSION

3.1 Variation of the Global Parameter $I_{0,\alpha}$ With Frequency

A convenient measure of the load on the upper surface is the chordwise integral of the unsteady-pressure distribution. As introduced in Ref. 19, this parameter is defined by

$$I_q(t) = \int_0^1 C_p(x,t)(x/c)^q \, d(x/c)$$

where $q = 0$ is a measure of the lift attributed to the upper surface (with sign reversed). A Fourier decomposition of $I_0(t)$ defines the amplitude of the first harmonic component

$$\alpha I_{0,\alpha} = \frac{1}{T} \int_0^T I_0(t)\exp(-i\omega t)dt$$

Considering first the attached flows, conditions 1-3 in Table 1, the variation of the magnitude of $I_{0,\alpha}$ with frequency is shown in Table 2, with Reynolds number as parameter. Values from subsonic, inviscid, unsteady aerodynamic theory (Ref. 21) are also shown for comparison. The frequency variation, typical of attached transonic flows — decreasing amplitude with increasing frequency — persists at all Reynolds numbers. The data also show decreasing amplitudes with increasing Reynolds numbers at most frequencies. For the subsonic flow ($M = 0.500$) the variations are minimal and can probably be accounted for by simple inclusion of the boundary-layer displacement. The transonic flows, being sensitive to shock-wave/boundary-layer interactions, show slightly more severe scale effects.

A graphic summary of the scale effect for conditions 1-3 is shown in Fig. 2 where the variation of the complex amplitude with Reynolds number is presented at a reduced frequency $k = 0.05$. As expected, the subsonic flow condition is least affected by Reynolds number. The trend for both the conventional and supercritical data at transonic Mach numbers is toward decreasing in-phase and out-of-phase (Re and Im) components with Reynolds number. It is noteworthy that, for each flow condition, the phase does not change by more than 5° over the Reynolds numbers range considered.

In Refs. 18 and 19 it was shown that the aerodynamic transfer function (variation of load with frequency) was not even qualitatively consistent with linear theory when the shock wave was strong enough to separate the boundary layer. The separated boundary layer had a major effect on the loads, and it is expected that scale effects would also be very important. Table 3 shows the magnitude of the complex amplitudes for conditions where strong unsteady shock-wave/boundary-layer interactions are encountered. No discernible trends are evident from these data. In fact, the magnitudes undergo alarming variations

with Reynolds number when compared with the attached-flow data. Due to this complex behavior, further information must be gleaned from the unsteady-pressure data itself.

3.2 Unsteady-Pressure Distributions

The first harmonic complex unsteady pressure is defined by the following expression:

$$\alpha C_{p,\alpha}(x) = \frac{1}{T}\int_0^T C_p(x,t)\exp(-i\omega t)dt$$

An analysis of the in-phase and out-of-phase (Re and Im) component of $C_{p,\alpha}$ will show that the distributions for attached-flow conditions are qualitatively consistent with the simplest theoretical models that include viscous effects by consideration of the boundary-layer displacement. The separated flow, however, shows important unsteady effects that are attributed to both the steady-flow scale effect and the unsteady viscous response of the boundary layer.

The data for attached-flow conditions 1-3 are shown in Figs. 3-5, respectively. For each frequency, the mean, in-phase, and out-of-phase components of the unsteady-pressure distribution are presented. Figure 3 shows that the subsonic flow ($\alpha = 0$, $M = 0.5$) has minimal scale effect. The only difference between Reynolds numbers is the slight dip in the in-phase component at wing station $x/c = 0.5$. Sublimation photographs showed that transition occurred at this location at $Re = 2.5 \times 10^6$; at $Re = 10 \times 10^6$, transition was very close to the leading edge. In any event, the state of the boundary layer has no effect on the unsteady-pressure distribution, which assumes the classical shape that was predicted many years ago from linearized subsonic theory. The same airfoil at transonic speeds in Fig. 4 ($\alpha = 0$, $M = 0.8$) shows that scale effect is also quite minimal. Aside from a slight upwind movement of the mean shock position that affects the chordwise location of the unsteady-pressure peak, the effect is minor. Sublimation photographs at this condition showed that transition occurs at the shock wave at $Re = 3.3 \times 10^6$; while leading-edge transition was observed at $Re = 12.6 \times 10^6$. The last attached flow condition, shown in Fig. 5 for the NLR 7301 supercritical airfoil, exhibits more severe scale effects. Although the region of rapid compression (probably not a shock wave at this supercritical design condition) moves only slightly, the unsteady pressure is quite different at the three Reynolds numbers indicated. These differences are probably due to the large extent of supercritical flow on the upper surface that is affected by the change in effective airfoil shape due to the unsteady boundary-layer growth. The difficulty in distinguishing differences by examining the integrated values shown previously is obvious because of the varying contribution to the loads from positive and negative lobes of the unsteady pressures.

The data for shock-induced separation are more difficult to analyze. These data are shown in Figs. 6 and 7. Figure 6 shows the large effect of Reynolds number for the NACA 64A010 at $\alpha = 4°$, $M = 0.8$ (condition 4 in Table 1). The mean flow differs not so much in the shock position as in the extent of separated flow downstream of the shock. This separated flow has a marked effect on the in-phase unsteady pressure at the shock wave and beyond. The out-of-phase pressures are not very much different at the two Reynolds numbers shown. The mechanisms whereby the in-phase pressures are more sensitive than the out-of-phase pressures have yet to be explained. Figure 7 shows similar data for the supercritical airfoil at a Mach number beyond its design point (condition 5 in Table 1). The mean flow differs from the previous case in the absence of any discernible training-edge pressure recovery downstream of the shock wave. This indicates a more severe flow separation. The data for the unsteady components of the pressure distribution also show a significant sensitivity to Reynolds number. For the in-phase component, especially, variations in the negative contribution to the load change rapidly with Reynolds number. This large variation gives rise to the confusing trends in the unsteady loads shown in Table 3. Again, it should be noted that the in-phase components appear to be more sensitive to Reynolds number than the out-of-phase components.

It is clear from the preceding discussion that a more fundamental data set needs to be examined to clarify the underlying physical mechanisms behind the scale effect. The final sequence of data will show how the Reynolds number effects the instantaneous unsteady-pressure time histories.

3.3 Instantaneous Pressure Data

The measured unsteady-pressure coefficients $C_p(x,t)$ are presented in Figs. 8 to 12 for the five flow conditions listed in Table 1. At each chordwise station (identified by a numerical key), data are shown at two Reynolds numbers. The mean portion of the instantaneous pressure coefficient was suppressed for clarity. (The reference line for each trace is the corresponding tic mark on the airfoil contour.) As explained in Ref. 20, the dynamic data have been processed to eliminate all asynchronous signals. Thus, all of the dips and bulges shown in the data are truly periodic. Whether they can be traced to a particular fluid-mechanical event at that instant is argumentative, but they are included here for completeness. The input motion is the same for both Reynolds numbers and can be used as the phase reference ($\omega t = 0$ when $\alpha = \alpha_{max}$). For the most part, data are shown at the low, reduced frequency $k = 0.05$.

The subsonic flow (condition 1) is presented in Fig. 8, and, as expected, scale effect is minimal. The usual trend of decreasing amplitude with increasing chordwise location is obvious. The distorted signal at $Re = 2.5 \times 10^6$ in traces 9 and 10 is apparently caused by the transitional boundary layer. The "noise" on traces 15 and 16 at low Reynolds number has no discernible fluid-mechanical origin.

The effect of increasing the Mach number to 0.80 is shown in Fig. 9. The presence of the shock wave is apparent by its distortion of the pressure signal of both Reynolds numbers, causing a severe local scale effect. However, both upstream and downstream of the shock wave, the Reynolds number does not have a significant effect. The global ramifications of these local effects were tabulated in Table 2.

Data from the supercritical airfoil at its shock-free design condition are shown in Figs. 10a and 10b. Data are presented at two frequencies to show the complicated cross-coupling between frequency and scale effects that was not present in the previous cases. In Fig. 10a data at the low reduced frequency of $k = 0.05$ show very significant scale effects in the supercritical flow region. At $Re = 12.6 \times 10^6$ there

is a higher amplitude, more distortion, and significant phase shifting. Whether these effects can be explained by simple boundary-layer displacement corrections remains to be answered. In Fig. 10b there is a surprising trend toward reduced harmonic distortions at higher Reynolds numbers (traces 5-9), although there are still significant phase shifts attributable to scale effect. At the "shock wave" (which appears during the cycle), the effect of Reynolds number is apparent. Consistent with the previous attached flow data, there is minimal response near the trailing edge at both frequencies.

Data pertaining to the second flow regime (e.g., shock-induced separation), are presented in Figs. 11 and 12. In Fig. 11 the scale effect is most prominent at the shock-wave location (traces 8 and 9). The fundamental frequency data shown in Fig. 6 indicate that the in-phase component is most severely affected by the Reynolds number. The large change in the unsteady pressure is apparent. Upstream, there is a significant increased phase lag with increasing Reynolds number. This phase lag persists into the separated-flow region aft of the shock. Unfortunately, no data are available at $k = 0.05$.

In Fig. 12 the well-separated flow over the supercritical airfoil does not induce large unsteady disturbances downstream of the shock. This seems to ameliorate the scale effect in the leading-edge region, but not at the shock itself. Data at $k = 0.05$ show similar trends.

This cursory examination of the unsteady-pressure traces indicates the sensitivity of the flow patterns to geometry, frequency, mean-flow conditions, and Reynolds number. It is clear that predictive schemes must include, as a minimum, physical models of all of these parameters.

4. CONCLUDING REMARKS

Examination of some of the data from a series of tests on oscillating airfoils in the Ames 11- by 11-Foot Transonic Wind Tunnel showed that scale effects could be a very important factor in the unsteady aerodynamic behavior of the airfoils. Configurations with mean flows that support fully attached boundary layers and weak shock waves have unsteady response characteristics that are mild functions of Reynolds number. These configurations can probably be modeled with currently available computational tools. An exception, perhaps, is airfoils that possess mean flows with extensive regions of supercritical flow. The detailed pressure distributions contain substantial scale effects, but the overall loads may not be so severely affected.

Configurations with mean flows having detached boundary layers are enigmatic. As reported in Refs. 18 and 19, the contribution to the unsteady load may be caused by a delicate balancing of positive and negative lobes in the unsteady pressures (see Fig. 7). For these conditions, shape changes caused by scale effects may have severe ramifications. The erratic behavior of the unsteady loads shown in Table 3 is illustrative of this effect. The major technological application of unsteady aerodynamics is to aeroelastic analysis and design. The sensitivity of flutter boundaries and stability margins to scale effects must be considered in those situations.

In the mathematical modeling of unsteady transonic aerodynamics, it is clear that the Reynolds number needs to be included as a primary parameter. Progress in computational research during the past decade was characterized by the inclusion of nonlinear thickness effects, and it is hoped that this and other experimental data, along with new computational efforts, will advance our knowledge well beyond the inviscid approximation.

REFERENCES

1. Ackeret, J.; Feldmann, F.; and Rott, N.: Investigations of Compression Shocks and Boundary Layers in Gases Moving at High Speed. NACA TM-1113, 1947.

2. Holder, D. W.: The Transonic Flow Past Two-Dimensional Airfoils. J. Royal Aero. Soc., vol. 68, Aug. 1964, pp. 501-516.

3. Pearcy, H. H.; Haines, A. B.; and Osborne, J.: The Interactions between Local Effects at the Shock and Rear Separation. Transonic Aerodynamics, AGARD CP-35, Sept. 1968, pp. 11-1 to 11-23.

4. Blackwell, J. A.: Effect of Reynolds Number and Boundary-Layer Transition Location on Shock-Induced Separations. Transonic Aerodynamics, AGARD CP-35, Sept. 1968, pp. 21-1 to 21-10.

5. Blackerby, W. T.; and Cahill, J. F.: High Reynolds Number Tests of a C-141A Aircraft Semispan Model to Investigate Shock-Induced Separation. NASA CR-2604, 1975.

6. Gessow, A.: NASA Research Objectives and Roles. Advanced Technology Airfoil Research, NASA CP-2045, 1979.

7. Ashley, H.; and Zartarian, G.: Thickness and Boundary-Layer Effects. AGARD Manual on Aeroelasticity, vol. II, Chap. 9., Nov. 1960.

8. Jones, W. P.: Trends in Unsteady Aerodynamics. J. Royal Aeronaut. Soc., vol. 67, no. 627, 1963, pp. 137-151.

9. McCroskey, W. J.: Some Current Research in Unsteady Fluid Dynamics. Trans. ASME. J. Fluids Eng., vol. 99, Mar. 1977, pp. 8-39.

10. Tijdeman, H.; and Seebass, R.: Transonic Flow Past Oscillating Airfoils. Annual Review of Fluid Mechanics, vol. 12, Annual Reviews Inc., Palo Alto, Calif., 1980, pp. 181-222.

11. Levy, L. L., Jr.: Experimental and Computational Steady and Unsteady Transonic Flows about a Thick Airfoil. AIAA J., vol. 16, June 1978, pp. 564-572.

12. Steger, J.: Implicit Finite-Difference Simulation of Flow About Arbitrary Two-Dimensional Geometrics. AIAA J., vol. 16, July 1978, pp. 679-686.

13. Steger, J.; and Bailey, H. E.: Calculation of Transonic Aileron Buzz. AIAA J., vol. 18, Mar. 1980, pp. 249-255.

14. Chyu, W.; and Davis, S.: Calculation of Unsteady Transonic Flow over an Arbitrary Airfoil. AIAA Paper 79-1554, Williamsburg, VA, July 1979.

15. Tijdeman, H.: Investigations of the Transonic Flow Around Oscillating Airfoils. NLR TR-77090U, Oct. 1977.

16. Grenon, R.; Desopper, A.; and Sides, J.: Unsteady Effects of a Control Surface in Two-Dimensional Subsonic and Transonic Flow. Aerodynamic Characteristics of Controls, AGARD CPP-262, May 1979, pp. 19-1 to 19-13.

17. Malcolm, G.; and Davis, S.: New NASA-Ames Wind Tunnel Techniques for Studying Airplane Spin and Two-Dimensional Unsteady Aerodynamics. Dynamic Stability Parameters, AGARD CP-235, Nov. 1978, pp. 3-1 to 3-12.

18. Davis, S.; and Malcolm, G.: Experiments in Unsteady Transonic Flow. AIAA Paper 79-769, St. Louis, MO, Apr. 1979.

19. Davis, S.; and Malcolm, G.: Unsteady Aerodynamics of Conventional and Supercritical Airfoils. AIAA Paper 80-734, Seattle, WA, May 1980.

20. Davis, S.: Computer/Experiment Integration for Unsteady Aerodynamic Research. Int. Congress on Instrumentation in Aerospace Simulation Facilities, ICIASF '79 Record, Sept. 1979, pp. 237-250.

21. Bispinghoff, R.; and Ashley, H.: Principles of Aeroelasticity. J. Wiley and Sons, New York, 1962, p. 106.

TABLE 1.- RANGE OF FLOW CONDITIONS CONSIDERED

Flow condition	Airfoil	M	α_m	Motion
1	NACA 64A010	0.500	0	Pitching ±1° at 0.25 c
2	NACA 64A010	0.796	0	Pitching ±1° at 0.25 c
3	NLR 7301	0.752	0.37	Pitching ±0.5° at 0.40 c
4	NACA 64A010	0.789	4.0	Pitching ±1° at 0.25 c
5	NLR 7301	0.807	0.38	Pitching ±0.5° at 0.40 c

TABLE 2.- MAGNITUDE OF UNSTEADY LOADING ATTRIBUTED TO UPPER SURFACE — ATTACHED FLOW

Re × 10^{-6}	Mag $I_{0,\alpha}$							
	k = 0	k = 0.025	k = 0.05	k = 0.10	k = 0.15	k = 0.20	k = 0.25	k = 0.30
Flow condition 1 (M = 0.500)								
2.5	3.7	3.67	3.59	3.27	2.97	2.83	-	-
5	3.8	-	-	-	-	2.45	-	-
10	-	-	3.43	3.19	2.91	2.74	2.58	-
Inviscid theory	3.64	3.42	3.22	2.91	2.69	2.52	2.44	2.38
Flow condition 2 (M = 0.796)								
3.3	5.5	-	4.87	-	3.19	2.84	2.24	-
6.7	5.7	-	-	-	-	2.67	-	-
12.6	-	4.62	4.41	3.80	2.90	2.68	2.16	2.16
Inviscid theory	5.25	4.61	4.12	3.46	3.07	2.84	2.71	2.63
Flow condition 3 (M = 0.752)								
3.3	-	-	6.46	-	-	2.98	-	-
6.2	-	6.56	6.19	4.80	-	3.67	-	2.01
11.5	-	6.05	5.62	4.63	3.65	3.12	-	1.94
Inviscid theory	4.76	4.28	3.88	3.22	2.97	2.75	2.62	2.54

TABLE 3.- MAGNITUDE OF UNSTEADY LOADING ATTRIBUTED TO UPPER SURFACE — SEPARATED FLOW

Re × 10^{-6}	Mag $I_{0,\alpha}$	
	k = 0.05	k = 0.20
Flow condition 4 (M = 0.789)		
6.2	-	4.48
11.9	1.67	5.57
Inviscid theory	4.12	2.84
Flow condition 5 (M = 0.807)		
3.3	2.39	1.53
6.3	0.44	0.69
11.7	1.08	0.88
Inviscid theory	4.13	2.82

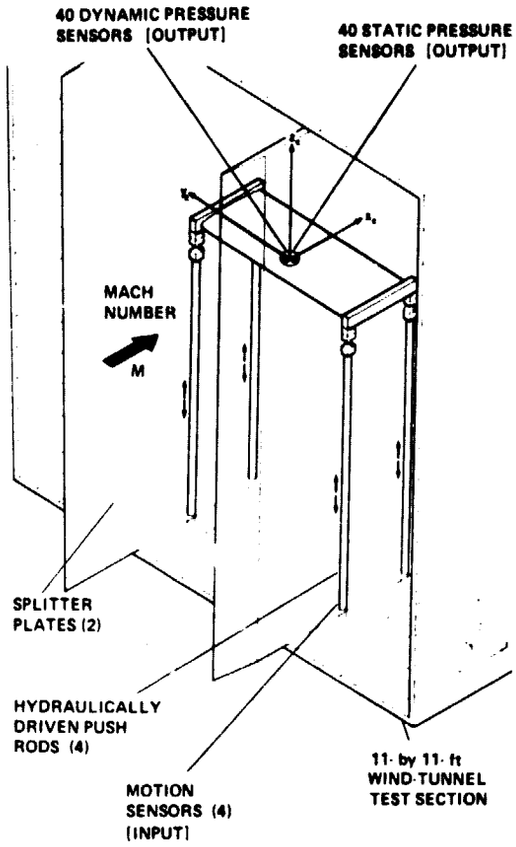

Fig. 1. Oscillating airfoil test apparatus installed in the 11- by 11-Foot (3.4 by 3.4 m) Transonic Wind Tunnel at Ames Research Center.

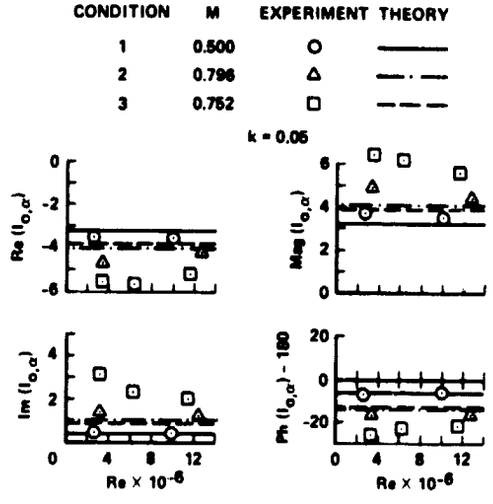

Fig. 2. Variation of the unsteady loading attributed to the upper surface with Reynolds number; low-frequency data, k = 0.05.

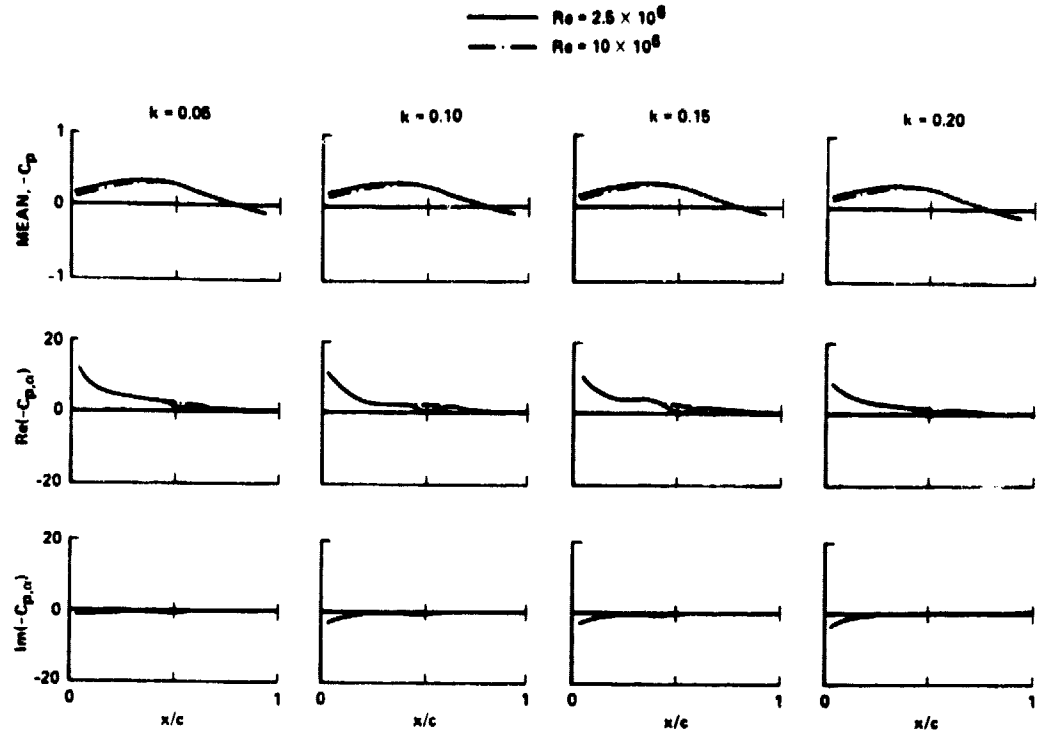

Fig. 3. Unsteady-pressure distribution on oscillating NACA 64A010 airfoil; mean and first harmonic component, M = 0.500, α_m = 0°, pitching ±1° at 0.25 c.

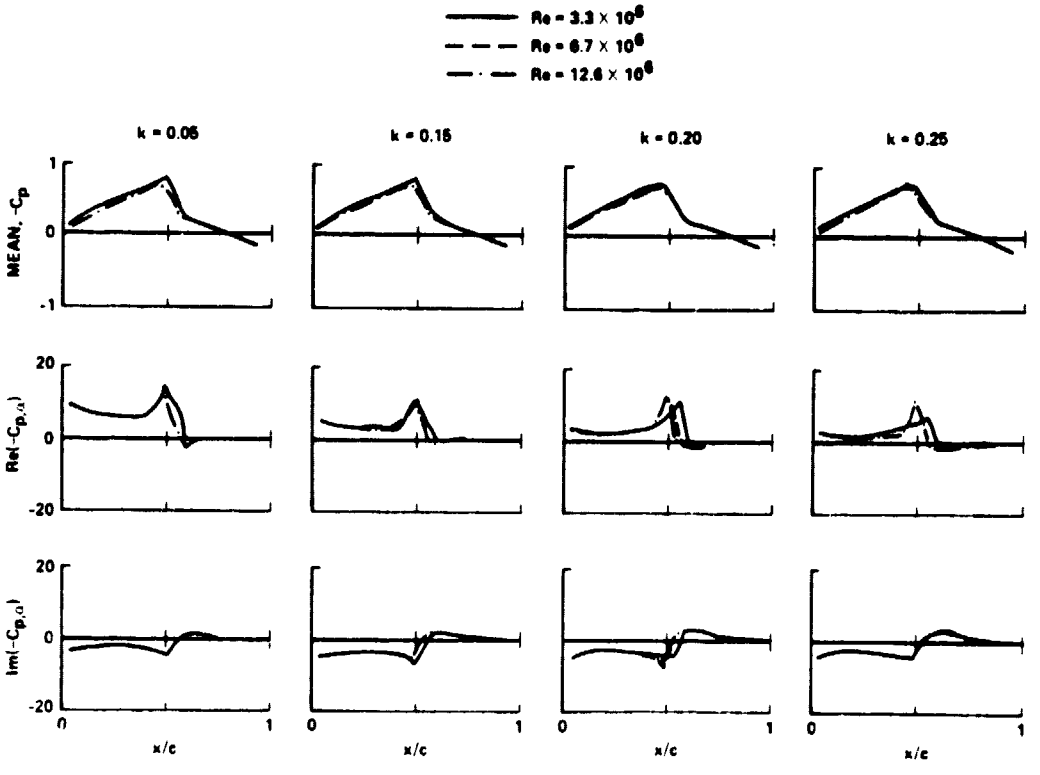

Fig. 4. Unsteady-pressure distribution on oscillating NACA 64A010 airfoil; mean and first harmonic component, M = 0.796, α_m = 0°, pitching ±1° at 0.25 c.

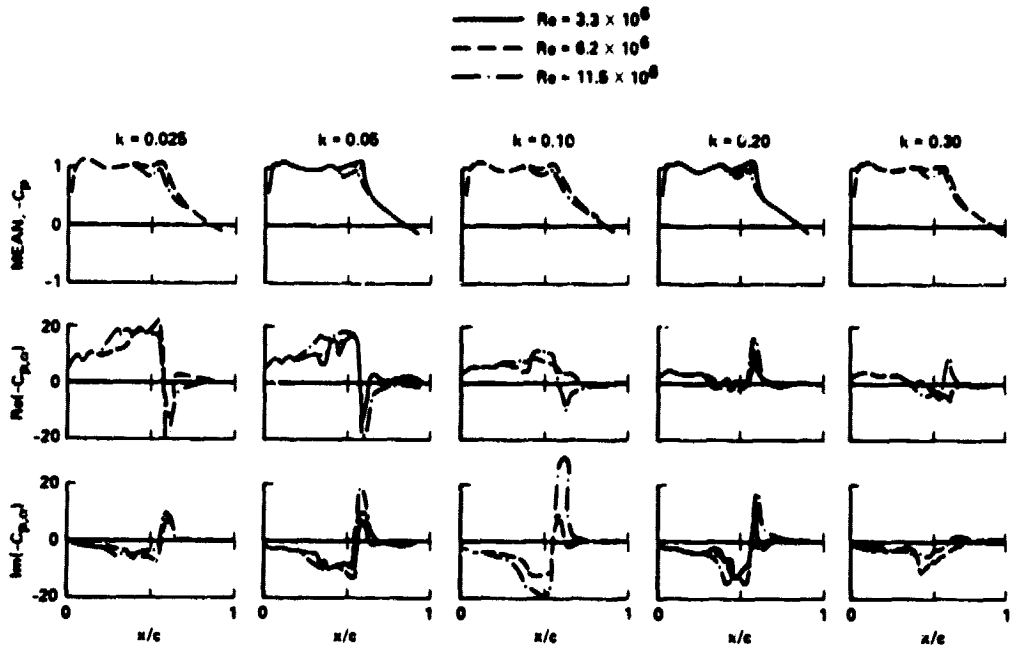

Fig. 5. Unsteady-pressure distribution on oscillating NLR 7301 airfoil; mean and first harmonic component, M = 0.752, α_m = 0.37°, pitching ±0.5° at 0.40 c.

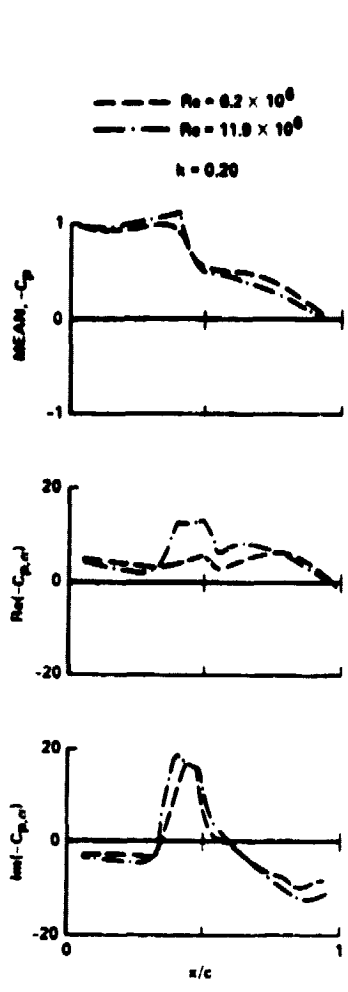

Fig. 6. Unsteady-pressure distribution on oscillating NACA 64A010 airfoil; mean and first harmonic component, M = 0.789, α_m = 4°, pitching ·1° at 0.25 c.

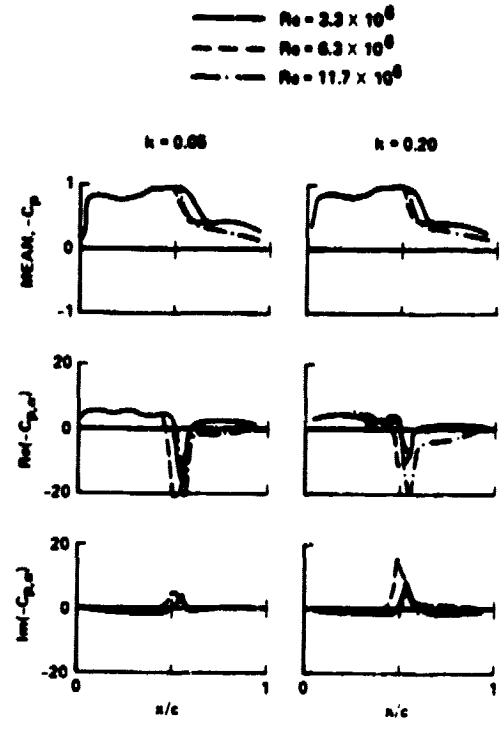

Fig. 7. Unsteady-pressure distribution on oscillating NLR 7301 airfoil; mean and first harmonic component, M = 0.807, α_m = 0.38°, pitching ±0.5° at 0.40 c.

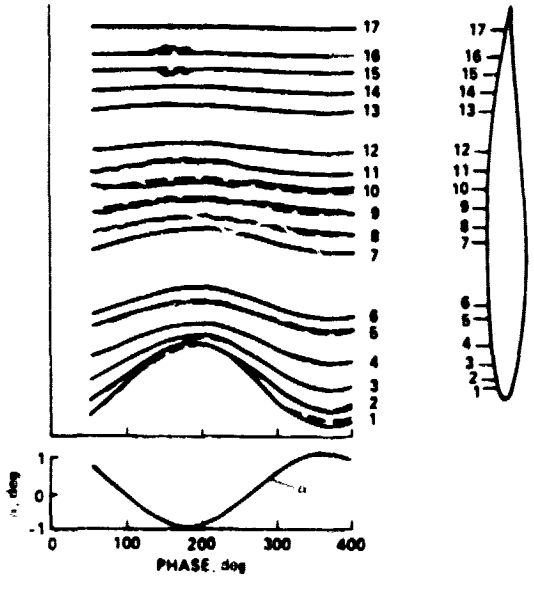

TRACE NO.	STATION x/c
1	0.033
2	0.082
3	0.091
4	0.140
5	0.200
6	0.243
7	0.402
8	0.440
9	0.488
10	0.538
11	0.584
12	0.633
13	0.733
14	0.781
15	0.829
16	0.872
17	0.941

Re = 2.5 · 10^6
Re = 10 · 10^6

Fig. 8. Complete time histories of unsteady-pressure data; M = 0.500, α_m = 0°, pitching ·1° at 0.25 c, k = 0.05.

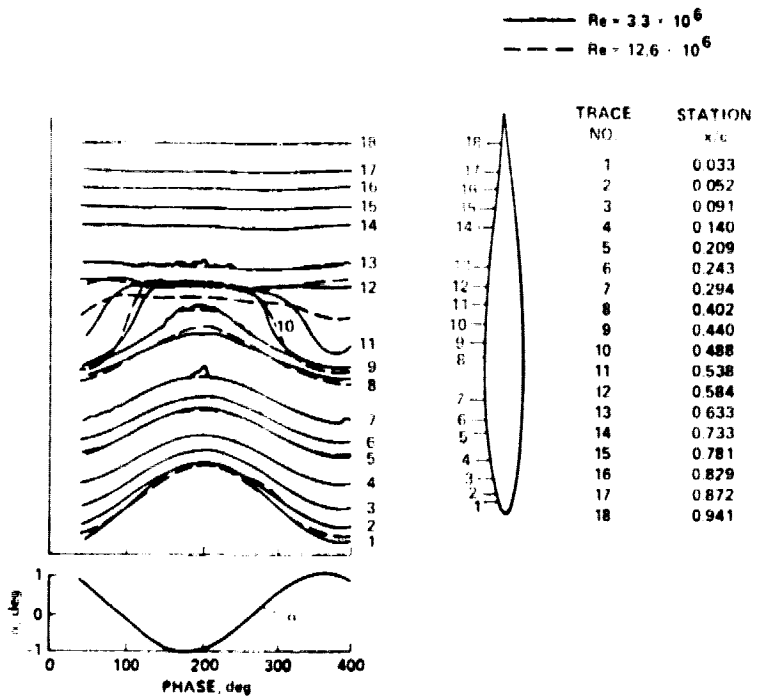

Fig. 9. Complete time histories of unsteady-pressure data; M = 0.796, α_m = 0°, pitching ±1° at 0.25 c, k = 0.05.

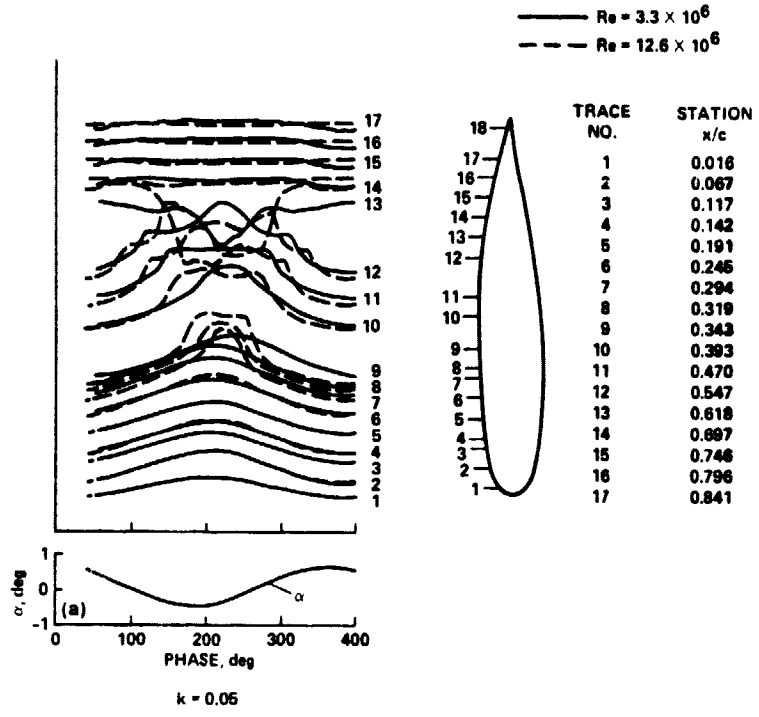

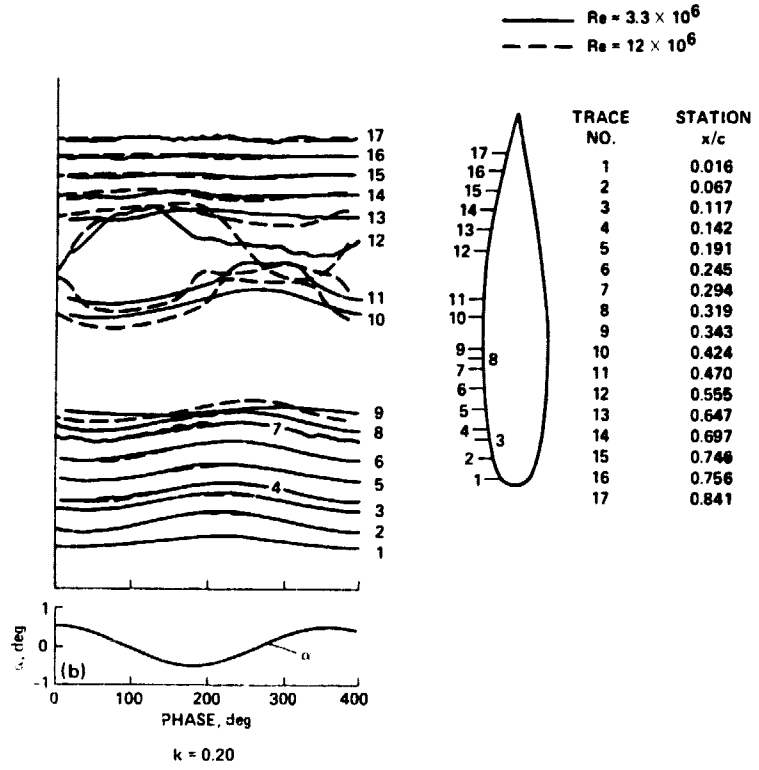

Fig. 10. Complete time histories of unsteady-pressure data; M = 0.752, α_m = 0.37°, pitching ±0.5° at 0.40 c.

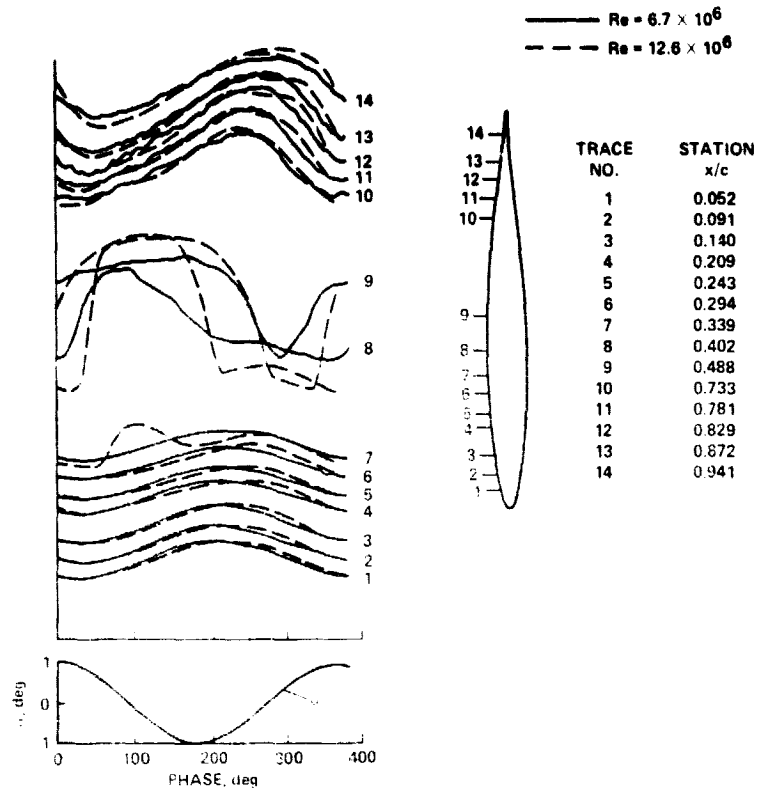

Fig. 11. Complete time histories of unsteady-pressure data; M = 0.789, α_m = 4°, pitching ±1° at 0.25 c, k = 0.20.

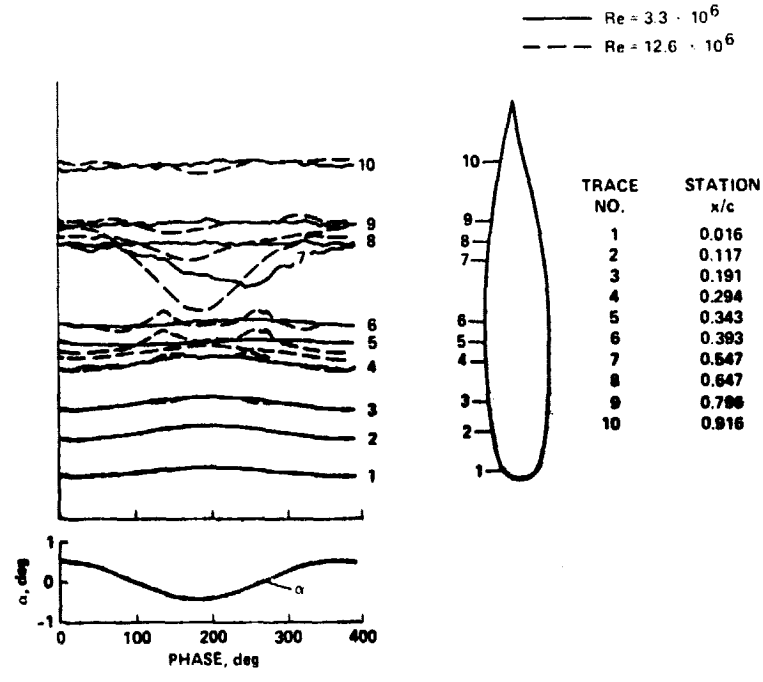

Fig. 12. Complete time histories of unsteady-pressure data; M = 0.807, α_m = 0.38°, pitching ±0.5° at 0.40 c, k = 0.20.